

Mutational Analysis of Substrate Interactions with the Active Site of Dialkylglycine Decarboxylase[†]

Emily J. Fogle[‡] and Michael D. Toney^{*,§}

[‡]Department of Chemistry and Biochemistry, California Polytechnic State University, San Luis Obispo, California 93407, and
[§]Department of Chemistry, University of California, Davis, California 95616

Received April 27, 2010; Revised Manuscript Received June 10, 2010

ABSTRACT: Pyridoxal phosphate (PLP)-dependent enzymes catalyze many different types of reactions at the α -, β -, and γ -carbons of amine and amino acid substrates. Dialkylglycine decarboxylase (DGD) is an unusual PLP-dependent enzyme that catalyzes two reaction types, decarboxylation and transamination, in the same active site. A structurally based, functional model has been proposed for the DGD active site, which maintains that R406 is important in determining substrate specificity through interactions with the substrate carboxylate while W138 provides specificity for short-chain alkyl groups. The mechanistic roles of R406 and W138 were investigated using site-directed mutagenesis, alternate substrates, and analysis of steady-state and half-reaction kinetics. Experiments with the R406M and R406K mutants confirm the importance of R406 in substrate binding. Surprisingly, this work also shows that the positive charge of R406 facilitates catalysis of decarboxylation. The W138F mutant demonstrates that W138 indeed acts to limit the size of the subsite C binding pocket, determining specificity for 2,2-dialkylglycines with small side chains as predicted by the model. Finally, work with the double mutant W138F/M141R shows that these mutations expand substrate specificity to include L-glutamate and lead to an increase in specificity for L-glutamate over 2-aminoisobutyrate of approximately 8 orders of magnitude compared to that of wild-type DGD.

Pyridoxal phosphate-dependent enzymes catalyze a wide variety of reaction types at the α -, β -, and γ -carbons of amine and amino acid substrates. Dunathan (1) hypothesized that pyridoxal phosphate-dependent enzymes maintain their reaction specificity through stereoelectronic effects. According to this hypothesis, a given enzyme maintains a specific orientation of the common external aldimine intermediate, aligning the scissile bond parallel to the p orbitals of the extended π system and thereby maximizing orbital overlap and resonance interactions with the activated bond. The binding constraints that control the orientation of the substrate in the active site contribute to both reaction specificity and substrate specificity. Thus, reaction specificity and substrate specificity are especially interrelated in pyridoxal phosphate-dependent enzymes.

This is particularly true for dialkylglycine decarboxylase (DGD),¹ which is an unusual PLP-dependent enzyme that catalyzes decarboxylation and transamination in the same active site in distinct half-reactions (Scheme 1). A functional active site model of DGD has been proposed (2) and validated (3). In this model,

there are three subsites. The A subsite, near Q52 and K272, is the stereoelectronically activated position in which bond breaking and making occur. The B subsite, near R406 and S215, can bind a carboxylate or an alkyl group, and the C subsite, near W138 and M141, can bind an alkyl group only and is less sterically tolerant than the B subsite (Figure 1). The model suggests R406 is important in determining substrate specificity through interactions with the substrate carboxylate while W138 maintains specificity for short-chain alkyl groups by limiting the size of the substrate side-chain binding pocket.

Herein, steady-state and half-reaction kinetics are presented for the R406M and R406K mutants, which confirm the importance of R406 in substrate binding. This work also demonstrates that R406 plays an unexpected role in decarboxylation catalysis. Results with the W138F mutant support the binding subsite model in which W138 limits the size of the C subsite binding pocket, providing specificity for 2,2-dialkylglycines with small side chains. Finally, work with the double mutant W138F/M141R shows that these mutations lead to an expansion of the substrate specificity to include L-glutamate as a decarboxylation substrate.

EXPERIMENTAL PROCEDURES

Materials and Preparation of Mutants. All chemicals were purchased from Sigma unless otherwise noted. The Quikchange site-directed mutagenesis protocol (Stratagene) was used to introduce the desired mutations. The pBTac (Boehringer Mannheim) plasmid containing the WT gene was used as a template for all reactions except for the W138F/M141R double mutant which used the same plasmid containing the W138F DGD gene. The following primer pairs were used to introduce the desired mutations, with the converted codon underlined: R406M, 5'-GGG CGG

[†]Supported by Grant GM54779 from the National Institutes of Health.

*To whom correspondence should be addressed. E-mail: mdtoney@ucdavis.edu. Fax: (530) 752-8995. Telephone: (530) 754-5282.

¹Abbreviations: DGD, 2,2-dialkylglycine decarboxylase; PLP, pyridoxal 5'-phosphate; AIB, 2-aminoisobutyric acid; TB, terrific broth; IPTG, isopropyl β -D-thiogalactoside; TEA, triethanolamine; AMS, D,L- α -methylserine; AMG, D,L- α -methylglutamate; 2°ADH, NADPH-dependent secondary alcohol dehydrogenase; SSDH, succinic semialdehyde dehydrogenase; DTT, dithiothreitol; OPA, o-phthalaldehyde; AC5C, 1-aminocyclopentane-1-carboxylic acid; AC6C, 1-aminocyclohexane-1-carboxylic acid; LDH, lactate dehydrogenase; YADH, yeast alcohol dehydrogenase; GABA, γ -aminobutyric acid; WT, wild-type DGD; GABA-AT, γ -aminobutyric acid aminotransferase.

Scheme 1

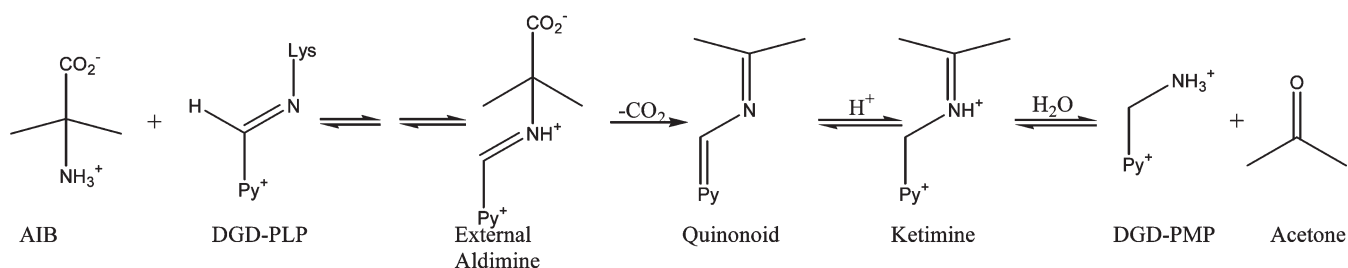
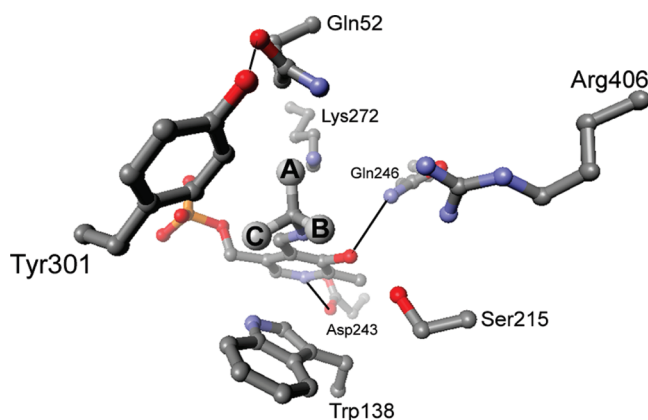
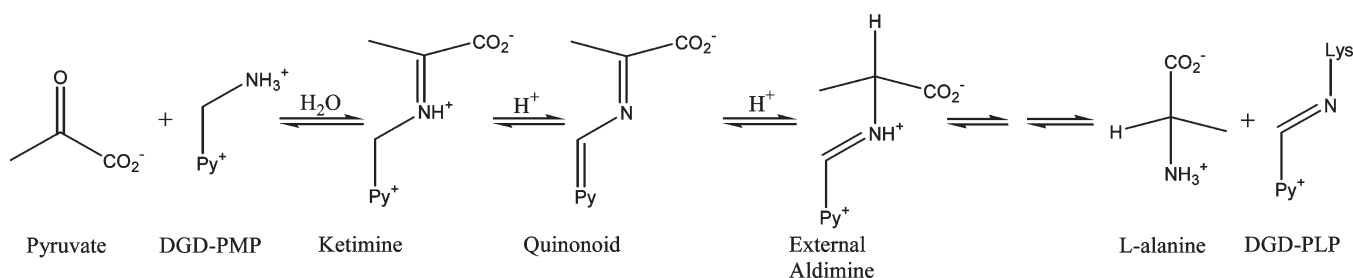
Decarboxylation Half-Reaction**Transamination Half-Reaction**

FIGURE 1: Active site structure of DGD showing the positions of the A, B, and C subsites of the functional model.

CGT GTT CAT GAT CGC GCC GCC GCT GAC G-3' and 5'-CGT CAG CGG CGG CGC GAT CAT GAA CAC GCC GCC C-3'; R406K, 5'-GGG CGG CGT GTT CAA AAT CGC GCC GCC GCT GAC G-3' and 5'-CGT CAG CGG CGG CGC GAT TTT GAA CAC GCC GCC C-3'; W138F, 5'-CGG CTT CGC GCA GTC GTT TCA CGG GAT GAC GGG-3' and 5'-CCC GTC ATC CCG TGA AAC GAC TGC GCG AAG CCG-3'; and W138F/M141R, 5'-CGT TTC ACG GGC GCA CGG GCG CGG CC-3' and 5'-GGC CGC GCC CGT GCG CCC GTG CCC CG-3'. Because of the high GC content of the DGD gene, it was necessary to use 5% (v/v) DMSO in polymerase chain reactions (PCRs). After transformation into *Escherichia coli* JM109 using standard procedures (4), the mutant plasmid was isolated using a commercial kit (Qiagen) and the full coding region sequenced to confirm that the desired mutation had been incorporated.

Expression and Purification of Mutants. For overexpression, 750 mL of TB was inoculated with a 5 mL overnight culture and grown at 37 °C until the OD₆₀₀ reached 0.4.

The cells were placed on ice for 20 min; expression was induced with 500 μM IPTG, and cell growth was continued at 33 °C for 8–10 h. The cells were pelleted by centrifugation, resuspended in lysis buffer [20 mM TEA-HCl (pH 7.8), 50 mM KCl, 20 μM PLP, and 1 M ammonium sulfate], and stored at -80 °C. The thawed cell suspension was sonicated and the cell debris removed by centrifugation. The cell free extract was brought to 2.2 M ammonium sulfate and stirred at 4 °C for 1 h and the precipitated protein removed by centrifugation. The pellet was dissolved and dialyzed into 20 mM TEA-HCl (pH 7.8) and 20 μM PLP, and the protein solution was loaded onto a 50 mL Q Sepharose Fast Flow column (Pharmacia). A gradient from 100 to 400 mM KCl in 20 mM TEA-HCl (pH 7.8) eluted protein. The fractions were analyzed by SDS-PAGE, and those containing DGD were pooled, concentrated, brought to 1 M in KCl, and loaded onto a 50 mL phenyl Sepharose column (Pharmacia). The protein was eluted with a gradient from 1 to 0 M KCl in 20 mM TEA-HCl (pH 7.8). The purest fractions, as judged by SDS-PAGE, were pooled, concentrated, and dialyzed into 50 mM TEA-succinate (pH 7.8), 50 mM dipotassium succinate, and 20 μM PLP. The protein was aliquoted, flash-frozen, and stored at -80 °C. The protein concentration was determined using both the extinction coefficient determined for DGD and the DC protein assay kit from Bio-Rad with IgG as a standard.

Steady-State Assays. Oxidative decarboxylation of 2-aminoisobutyric acid (AIB), D,L-α-methylserine (AMS), and D,L-α-methyl glutamate (AMG) was followed by coupling the ketone produced to the 2°ADH reaction as previously described (3). Loss of NADPH absorbance at 340 nm was followed on a Kontron UVIKON 9420 instrument. Reaction mixtures contained 100 mM TEA-succinate (pH 7.8), 100 mM dipotassium succinate, 1 unit/mL 2°ADH, 20 μM PLP, and 300 μM NADPH. Stock solutions of all substrates were prepared in 20 mM TEA-succinate, and the pH of the solution was adjusted to 7.8. Pyruvic acid was titrated

to pH 7.8 with TEA and used as the α -keto acid substrate unless otherwise noted. For assays using AMS or AMG, the ketone product of oxidative decarboxylation was tested and confirmed to be a substrate for 2°ADH. Additionally, it was confirmed that the rate of decarboxylation was linearly dependent on DGD concentration for these assays. Initial rates were plotted versus substrate concentration and fitted to the Michaelis–Menten equation.

Oxidative decarboxylation of D- or L-glutamate to produce succinic semialdehyde was followed using the NADP-dependent succinic semialdehyde dehydrogenase (SSDH) reaction, monitoring the increase in NADPH absorbance at 340 nm as previously described (5). The reaction mixtures contained 30 mM TEA-succinate (pH 7.8), 50 mM dipotassium succinate, 5 mM DTT, 1 mM EDTA, 20 μ M PLP, 500 μ M NADP⁺, 5 mM α -ketoglutarate, and 3 units/mL SSDH. Initial rates were plotted versus substrate concentration and fitted to the Michaelis–Menten equation.

R406M and R406K Steady-State Kinetics. The steady-state kinetic parameters, k_{cat} , K_{AIB} , and K_{pyr} , were determined using the 2°ADH-coupled assay. Briefly, one substrate was held near saturation while the other varied. It was not possible to fully saturate R406M with AIB or AMS because of the solubility limits of these compounds and the large K_{m} values.

Nonoxidative Decarboxylation End-Point Assays for R406M. Assays to identify the amine products of nonoxidative decarboxylation were performed using a previously reported HPLC-based method (6). Reactions with 100 mM TEA-succinate (pH 7.8), 100 mM dipotassium succinate, 20 μ M PLP, 53 mM pyruvate, 10 μ M R406M, and either 500 mM AIB or 133 mM L-alanine were allowed to proceed at 25 °C for 12–16 h. The protein was denatured by addition of 2 μ L of glacial acetic acid to the 200 μ L reaction mixture, and the precipitated protein was removed by centrifugation. The reaction mixture was then derivatized with *o*-phthalaldehyde (OPA) prior to HPLC analysis. Briefly, a 100 μ L sample was mixed with 100 μ L of freshly prepared OPA reagent [4 mg of solid OPA, mixed with 4.5 mL of 0.1 M borate (pH 10.4), 15 μ L of 30% (v/v) Brij-35 detergent, and 10 μ L β -mercaptoethanol], allowed to react for 1 min at room temperature, and then acidified with 2 M acetic acid to pH 4.5. The derivatized sample was immediately run on a Hibar LiChrosorb C18 column using an Agilent 1100 HPLC system connected to a Perkin-Elmer 650-15 fluorescence detector. The HPLC method (6) used 50 mM sodium acetate (pH 5.7) and 5% (v/v) THF (solvent A), methanol (solvent B), or acetonitrile (solvent C). The elution gradient was as follows: 90% A and 10% B to 35% A and 65% B from 0 to 15 min, 35% A and 65% B from 15 to 20 min, 35% A and 65% B to 50% B and 50% C from 20 to 25 min, and 50% B and 50% C from 25 to 30 min. The flow rate was 1 mL/min, and the products were monitored using fluorescence (excitation at 340 nm, emission at 455 nm).

Stopped-Flow Multiwavelength Analysis of the AIB Decarboxylation Half-Reaction in R406M. The AIB decarboxylation half-reaction was followed by rapidly mixing PLP enzyme [in 20 μ M enzyme in 50 mM TEA-succinate (pH 7.8), 50 mM dipotassium succinate, and 20 μ M PLP] against an AIB solution prepared in the same buffer in an Applied Photophysics SX.18MV-R stopped-flow spectrometer. Coenzyme spectral changes were followed from 200 to 800 nm using a diode array detector. The data from 300 to 600 nm were globally fit using Specfit. A four-exponential model was used for the R406M data.

The apparent rate constants were fitted to eq 1 for the first process seen in R406M.

$$k_{\text{obs}} = \frac{k_{\text{max}}[\text{AIB}]}{K_{\text{app}} + [\text{AIB}]} + \text{offset} \quad (1)$$

Spectral Analysis of R406M Decarboxylation Half-Reactions with AC5C and AC6C. Coenzyme spectral changes from 300 to 600 nm were followed using a Hewlett-Packard 8453 UV–vis spectrophotometer. Reaction mixtures consisted of 50 mM TEA-succinate (pH 7.8), 50 mM dipotassium succinate, 20 μ M PLP, 20 μ M enzyme, and varying concentrations of 1-aminocyclopentane-1-carboxylate (AC5C) or 1-aminocyclohexane-1-carboxylate (AC6C). The multiwavelength data for both substrates were globally fitted to a two-exponential model using Specfit. The apparent rate constants obtained were plotted versus substrate concentration and fitted to eq 1.

Analysis of Products of the R406M Reaction with L-Alanine. Lactate dehydrogenase (LDH) was used to test for pyruvate resulting from transamination of L-alanine. Reaction mixtures consisted of 100 mM TEA-succinate (pH 7.8), 100 mM dipotassium succinate, 20 μ M PLP, 20 μ M R406M, and 150 mM L-alanine. The reaction mixture was incubated at 25 °C for 12 h, at which time 2 units/mL LDH and 300 μ M NAD⁺ were added, and the reaction was monitored for an increase in absorbance indicating the formation of pyruvate. A negative control without enzyme showed that no appreciable amount of pyruvate formed due to nonenzymatic transamination under these conditions.

An end-point assay using yeast alcohol dehydrogenase (YADH) was used to test for acetaldehyde, the product of oxidative decarboxylation of L-alanine. Reaction mixtures consisted of 100 mM TEA-succinate (pH 7.8), 100 mM dipotassium succinate, 20 μ M PLP, 20 μ M R406M, 53 mM pyruvate, and 100 mM L-alanine. The reaction mixture was incubated at 25 °C for 12 h, at which time 2 units/mL YADH and 200 μ M NADH were added, and the reaction was monitored for a decrease in absorbance due to formation of acetaldehyde. A negative control without enzyme was included. Any change in absorbance significantly greater than that observed in the negative control was used to estimate the upper limit for activity with the substrate.

An HPLC end-point assay was used to identify ethylamine, the product of nonoxidative decarboxylation of L-alanine. The reaction mixture was prepared as described above for the oxidative decarboxylation end-point assay. After incubation, the enzyme was denatured with acid and removed by centrifugation. The sample was subsequently derivatized with OPA and run on the HPLC system as described above. A negative control without enzyme was included to determine any nonenzymatic decarboxylation.

W138F Steady-State Kinetics. The values of k_{cat} , and the K_{m} values for AIB (K_{AIB}) and pyruvate (K_{pyr}), were determined using the 2°ADH-coupled assay as described above. K_{AIB} and K_{pyr} were determined by holding the pyruvate concentration at 50 μ M ($\sim 10K_{\text{pyr}}$) and the AIB concentration at 200 mM ($\sim 5K_{\text{AIB}}$). Studies that aimed to determine the catalytic efficiency of W138F with α -keto acids of varying side-chain lengths used pyruvate, α -ketobutyrate, α -ketovalerate, and α -ketocaproate. In these assays, the AIB concentration was held at 200 mM ($5K_{\text{AIB}}$) and the concentration of α -keto acid was varied. The data were fitted to the Michaelis–Menten equation.

Inhibition studies with D-phenylglycine were performed using a saturating pyruvate concentration and holding the concentration

Table 1: Steady-State Kinetic Parameters for R406 Mutants^a

	AIB				AMS			
	k_{cat} (s ⁻¹)	K_{AIB} (mM)	K_{pyr} (mM)	$k_{\text{cat}}/K_{\text{AIB}}$ (M ⁻¹ s ⁻¹)	k_{cat} (s ⁻¹)	K_{ams} (mM)	K_{pyr} (mM)	$k_{\text{cat}}/K_{\text{ams}}$ (M ⁻¹ s ⁻¹)
R406M	0.22 (0.02)	360 (61)	3.5 ^b (0.5)	0.6 (0.1)	0.074 (0.004)	452 (73)	3.7 (0.6)	0.16 (0.03)
R406K	1.6 (0.1)	33 (6)	8.8 (0.8)	49 (9)	0.76 (0.05)	62 (11)	6.7 (1.1)	12 (2)
WT	17.7 (0.5) ^c	2.2 (0.2)	0.098 (0.008)	8000 (800)	4.00 (0.09)	4.5 (0.3)	not determined	890 (60)

^aErrors are given in parentheses. ^b K_{pyr} was determined for the slow form of R406M DGD. ^cWT values for reaction with AIB taken from ref 16.

of AIB at K_{AIB} (40 mM). The data were fitted assuming competitive inhibition (eq 2), as previously observed with WT (3).

$$v_i = \frac{V_{\text{max}}[S]}{K_m(1 + [I]/K_i) + [S]} \quad (2)$$

End-Point Assays with W138F. W138F was tested for decarboxylation activity with D- and L-phenylglycine using end-point assays coupling the L-alanine formed from the reaction to L-alanine dehydrogenase. Reaction mixtures consisted of 100 mM TEA-succinate (pH 7.8), 100 mM dipotassium succinate, 1 mM pyruvate, 20 μ M PLP, 28 μ M W138F, and 10 mM D- or L-phenylglycine. The reaction mixtures were incubated at 25 °C for 12 h, at which time 300 μ M NAD⁺ and 2 units/mL L-alanine dehydrogenase were added, and the reaction was monitored for an increase in absorbance indicating the formation of L-alanine. In all cases, a sample without enzyme was included as a negative control.

Spectral Analysis of W138F Decarboxylation of L-Phenylglycine. Coenzyme spectral changes from 300 to 600 nm were followed as described above for the spectral analysis of AC5C and AC6C decarboxylation. Reaction mixtures consisted of 100 mM TEA-succinate (pH 7.8), 100 mM dipotassium succinate, 20 μ M PLP, 20 μ M W138F, and varying concentrations of L-phenylglycine. A two-exponential model using Specfit best fit the data.

Steady-State Kinetics with W138F/M141R. The reaction with AIB using the 2°ADH-coupled assay gave the steady-state kinetic parameters k_{cat} and K_{AIB} . K_{pyr} was not determined. Instead, it was assumed that K_{pyr} in W138F/M141R is essentially the same as in W138F, as observed for K_{AIB} . When K_{AIB} was being determined, pyruvate was held at a saturating concentration (1 mM) based on the K_{pyr} for W138F. The SSDH-coupled assay was used to study activity with L-glutamate. Reaction mixtures consisted of 30 mM TEA-succinate (pH 7.8), 50 mM dipotassium succinate, 5 mM DTT, 1 mM EDTA, 20 μ M PLP, 500 μ M NADP⁺, 5 mM α -ketoglutarate, 3 units/mL SSDH, and varying concentrations of L-glutamate.

Inhibition studies with D-glutamate and AMG were performed using the 2°ADH-coupled assay with AIB decarboxylation. Pyruvate was used at a saturating concentration, and the AIB concentration was held at K_{AIB} (40 mM) while the concentration of inhibitor varied. The data were fitted assuming competitive inhibition using eq 2.

End-Point Assays with D- and L-Glutamate. Decarboxylation of D- and L-glutamate in WT, W138F, and W138F/M141R was studied using the SSDH-coupled assay. Reaction mixtures consisted of 100 mM TEA-succinate (pH 7.8), 100 mM dipotassium succinate, 20 μ M PLP, and 1 mM α -ketoglutarate. D- and L-glutamate concentrations were held at 250 mM while 20 μ M W138F, 45 μ M W138F/M141R, or 5 μ M WT was used. Samples were incubated at 25 °C for 12–16 h, at which time 5 mM DTT,

1 mM EDTA, 500 μ M NADP⁺, and 3 units/mL SSDH were added. The reactions were monitored for an increase in absorbance indicating the formation of succinic semialdehyde resulting from oxidative decarboxylation of glutamate. In all cases, a negative control without enzyme was also included. Any change in absorbance significantly greater than that observed in the negative control was used to estimate the upper limit for activity with the substrate.

Nonoxidative Decarboxylation End-Point Assays for W138F/M141R. Nonoxidative decarboxylation of D- or L-glutamate to form γ -aminobutyric acid (GABA) was monitored using HPLC, using the method described above. Reaction mixtures consisted of 100 mM TEA-succinate (pH 7.8), 100 mM dipotassium succinate, 20 μ M PLP, 1 mM α -ketoglutarate, and 200 mM D- or L-glutamate. The 200 μ L reaction mixture was incubated at 25 °C for 12–16 h, after which enzyme was denatured with 2 μ L of glacial acetic acid and removed by centrifugation. The sample was derivatized with OPA and analyzed using the HPLC method described above. Negative controls without enzyme were included to check for background decarboxylation.

RESULTS

R406M and R406K Steady-State Kinetics. The steady-state kinetic parameters are listed in Table 1. Both mutants display nonlinear kinetic traces indicative of a fast enzyme form that converts to a slow form, as observed previously with WT (7). The data presented are for the fast form of the enzyme, with the exception of K_{pyr} for R406M which was determined for the slow enzyme form because of the experimental difficulty of determining this parameter for the fast enzyme form. The R406M mutant shows an 80-fold decrease in k_{cat} relative to WT, while k_{cat} in R406K decreases only 10-fold. The K_m values for AIB and pyruvate have increased. In R406M, K_{AIB} is 100-fold larger than for WT, while K_{pyr} shows a smaller increase of ~35-fold. As expected, substrate binding in R406K is not weakened to the degree seen in R406M; K_{AIB} increases ~10-fold, while K_{pyr} increases ~80-fold in R406R. HPLC analysis of the reaction products finds that R406M does not nonoxidatively decarboxylate AIB to form isopropylamine (data not shown).

The mutants using AMS as a substrate show trends in k_{cat} and K_m similar to those observed with AIB. With AMS as a substrate, the fast and slow forms of the enzyme are not observed. The rate decreases approximately 55-fold in R406M and 5-fold in R406K compared to that of WT, while K_{ams} increases 100-fold for R406M and 14-fold for R406K. These results suggest that R406 interacts strongly with both amino and keto acid substrates by forming a hydrogen bond or salt bridge to their carboxylate groups, as expected on the basis of X-ray crystallographic structures (8). The decrease in the decarboxylation rate constant, however, is unexpected and suggests that R406 plays a direct role in the decarboxylation half-reaction in addition to substrate binding.

The decarboxylation half-reaction with the cyclic substrates, AC5C and AC6C, was investigated in R406M using the spectral changes of the PLP cofactor. The spectral changes were fitted to a one-exponential equation for both substrates. This fitting (Figure 2) gave k_{\max} and the apparent dissociation constant, K_{app} (Table 2). The rate of decarboxylation for these substrates decreases significantly, 10^5 -fold for AC5C and 4600-fold for AC6C compared to that of WT. The apparent dissociation constants are slightly increased for the substrates: ~ 4 -fold for AC5C and ~ 3 -fold for AC6C.

Spectral Analysis of the AIB Decarboxylation Half-Reaction in R406M. The spectral changes seen in the AIB decarboxylation half-reaction in R406M are complex and ascribed to a serial four-step model (data not shown). Although the spectral changes are complex and the exact chemical nature of each process is not clear, fitting the concentration dependence of the apparent rate constants shows clearly that the decarboxylation

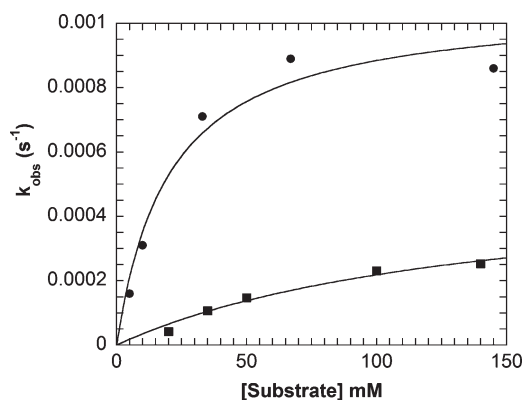


FIGURE 2: Concentration dependence of the observed rate constant for the decarboxylation half-reaction with AC5C (●) and AC6C (■) in R406M obtained from analysis of multiwavelength data. The lines represent fits to the Michaelis–Menten equation. Experimental mixtures consisted of 20 μM enzyme, 100 mM TEA-succinate (pH 7.8), 100 mM dipotassium succinate, 20 μM PLP, and varying concentrations of AC5C or AC6C.

Table 2: Kinetic Parameters for Alternate Substrates^a

	AC5C		AC6C	
	k_{\max} (s^{-1})	K_{app} (mM)	k_{\max} (s^{-1})	K_{app} (mM)
R406M	$9.4 (0.9) \times 10^{-4}$	15 (6)	$5 (1) \times 10^{-4}$	140 (50)
WT ^b	$0.98 (0.03)^c$	4.0 (0.8)	$2.3 (0.2)^c$	53 (150)

^aErrors are given in parentheses. ^bWT values taken from ref 3. ^cThe values given for WT are steady-state k_{cat} and K_{m} values; we assume that the decarboxylation half-reaction is rate-limiting in WT for AC5C and AC6C, so that $k_{\text{cat}} = k_{\max}$.

Table 3: Steady-State Kinetic Parameters for Binding and Oxidative Decarboxylation of Alternate Substrates in W138F Mutants^a

	D-glutamate		L-glutamate		AIB			$k_{\text{cat}}/K_{\text{L-Glu}} \cdot k_{\text{cat}}/K_{\text{AIB}}$
	K_{i}^b (mM)	k_{cat} (s^{-1})	$K_{\text{L-Glu}}$ (mM)	$k_{\text{cat}}/K_{\text{L-Glu}}$ ($\text{M}^{-1} \text{s}^{-1}$)	k_{cat} (s^{-1})	K_{AIB} (mM)	$k_{\text{cat}}/K_{\text{AIB}}$ ($\text{M}^{-1} \text{s}^{-1}$)	
W138F/M141R	89 (10)	0.0022 (0.0003)	270 (74)	0.008 (0.002)	0.0040 (0.0002)	41 (5)	0.10 (0.01)	0.08
W138F		4×10^{-6c}			0.179 (0.007)	37 (4)	4.8 (0.6)	
WT	>500	6×10^{-6c}	480 ^d (40)	8×10^{-6}	17.7 ^e (0.5)	2.2 ^e (0.2)	8000 ^e (800)	1×10^{-9}

^aErrors are given in parentheses. ^b K_{i} was determined assuming competitive inhibition against AIB in the AIB decarboxylation reaction. ^cBased on the total absorbance change observed in the SSDH end-point assay. ^dThe K_{m} value reported is the K_{i} obtained assuming competitive inhibition against AIB. ^eData for WT AIB decarboxylation taken from ref 16.

half-reaction in R406M is not rapid. For example, the kinetic parameters for the fastest process, for which the spectral changes are consistent with decarboxylation to form the PMP form of the enzyme, are as follows: $k_{\max 1} = 0.46 \pm 0.04 \text{ s}^{-1}$, and $K_{\text{app}1} = 800 \pm 160 \text{ mM}$. These are in reasonably good agreement with the steady-state values found for the fast enzyme form of R406M: $k_{\text{cat}} = 0.22 \pm 0.02 \text{ s}^{-1}$, and $K_{\text{AIB}} = 360 \pm 61 \text{ mM}$.

Analysis of the Products of the R406M Reaction with L-Alanine. The products of the reaction with L-alanine were investigated using several assays. Assays using lactate dehydrogenase showed clearly that pyruvate from transamination of L-alanine was formed when R406M was incubated with L-alanine. Assays using YADH were used to evaluate if R406M catalyzed the oxidative decarboxylation of L-alanine to acetaldehyde. Even after 12 h, there was no formation of acetaldehyde under the conditions tested. To exclude the possibility that R406M catalyzes nonoxidative decarboxylation of L-alanine, HPLC analysis was performed. Under no conditions was ethylamine, the product of nonoxidative decarboxylation, observed. Together, these results show that R406M is capable of catalyzing only the transamination of L-alanine and that no decarboxylation occurs with this substrate. Again, this implies an important role for R406 specifically in decarboxylation since WT can decarboxylate alanine (3).

W138F Steady-State Kinetics. The steady-state kinetic parameters for W138F are listed in Table 3. W138F shows an ~ 100 -fold decrease in k_{cat} compared to that of WT, while K_{AIB} increases approximately 20-fold. In W138F, the catalytic efficiency ($k_{\text{cat}}/K_{\alpha\text{-keto acid}}$) decreases approximately 1 order of magnitude as the side-chain length of the α -keto acid increases from one carbon (pyruvate) to four carbons (α -ketocaproate). In WT, $k_{\text{cat}}/K_{\alpha\text{-keto acid}}$ decreases 3 orders of magnitude (Figure 3) over the same range (3). Figure 3 plots the logarithm of $k_{\text{cat}}/K_{\alpha\text{-keto acid}}$ versus the number of side-chain carbons; the former corresponds to the free energy of activation for the reaction of free PMP enzyme with α -keto acid, while the latter is expected to be a measure of the energy of interaction of the α -keto acid side chain with the C subsite. The negative correlation implies that repulsive interactions between the α -keto acid side chain and the C subsite raise the free energy of activation as the size of the α -keto acid is increased.

W138F can decarboxylate L-phenylglycine, as observed for WT (3). End-point assays using L-alanine dehydrogenase (to detect alanine formed from pyruvate in the reaction mixture) show L-phenylglycine undergoes oxidative decarboxylation (data not shown). The reactivity with D-phenylglycine is quite different. In contrast to WT, which shows no inhibition by D-phenylglycine (3), W138F is inhibited by D-phenylglycine ($K_{\text{i}} = 50 \text{ mM}$). The inhibition observed was not due to pH or salt effects.

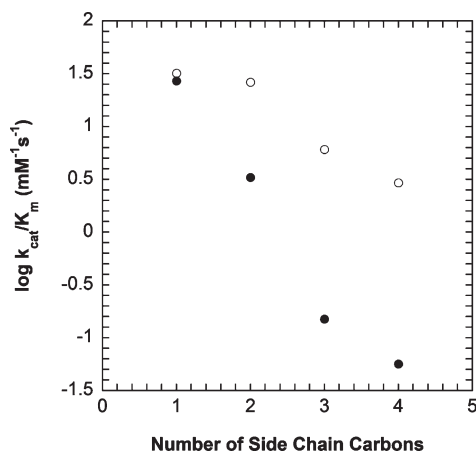


FIGURE 3: Rate constants for oxidative decarboxylation of AIB using α -keto acids with linear side chains one to four carbons in length for WT (●) and W138F (○). Experimental mixtures consisted of 100 mM TEA-succinate (pH 7.8), 100 mM dipotassium succinate, 200 mM AIB, 20 μ M PLP, 1 unit/mL 2°ADH, and 300 μ M NADPH.

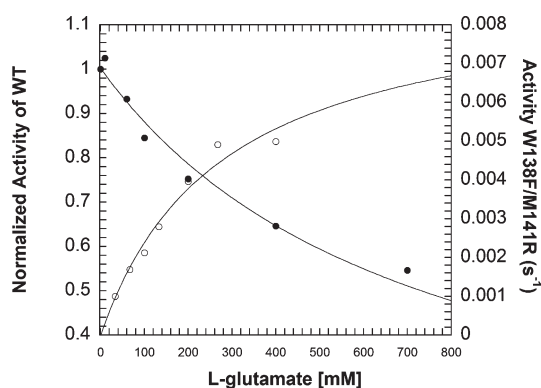


FIGURE 4: Comparison of inhibition of WT by L-glutamate (●) and activity in the W138F/M141R mutant (○). The lines represent fits to eq 2 for WT and the Michaelis–Menten equation for W138F/M141R. Experimental mixtures for WT consisted of 100 mM TEA-succinate (pH 7.8), 100 mM dipotassium succinate, 20 mM AIB, 2 mM pyruvate, 20 μ M PLP, 1 unit/mL 2°ADH, 300 μ M NADPH, and varying concentrations of L-glutamate. Experimental mixtures for W138F/M141R consisted of 30 mM TEA-succinate (pH 7.8), 50 mM dipotassium succinate, 5 mM DTT, 1 mM EDTA, 20 μ M PLP, 500 μ M NADP⁺, 5 mM α -ketoglutarate, 3 units/mL SSDH, and varying concentrations of L-glutamate.

Steady-State Kinetics of W138F/M141R. The steady-state kinetic parameters for W138F/M141R with AIB, L-glutamate, and D-glutamate are listed in Table 3. For the reaction with AIB, the double mutant shows an \sim 4000-fold decrease in k_{cat} relative to that of WT but only an \sim 45-fold decrease relative to that of W138F. The apparent dissociation constant for AIB remains essentially the same for the double mutant as for W138F, increasing \sim 20-fold relative to that of WT.

W138F/M141R catalyzes oxidative decarboxylation of L-glutamate (Figure 4). The rate of L-glutamate decarboxylation increases approximately 550-fold compared to those of WT and W138F. The parameters for W138F/M141R are as follows: $k_{\text{cat}} = 0.0022 \pm 0.0003 \text{ s}^{-1}$, and $K_{\text{L-Glu}} = 270 \pm 74 \text{ mM}$. Although WT does not catalyze decarboxylation of L-glutamate at a rate sufficiently fast to fully characterize the reaction, inhibition by L-glutamate of AIB decarboxylation can be assessed. The inhibition constant (K_i) for L-glutamate with WT is $480 \pm 40 \text{ mM}$ (Figure 4). HPLC assays show that a small amount of nonoxidative

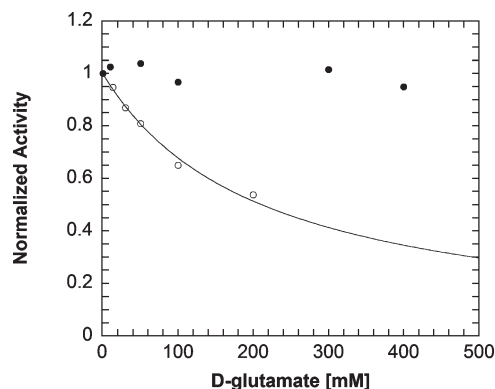


FIGURE 5: Comparison of inhibition of WT (●) and W138F/M141R (○) by D-glutamate. The line represents a fit to eq 2. Inhibition studies were performed using the 2°ADH-coupled assay with AIB decarboxylation. Pyruvate was used at a saturating concentration, and AIB was held at K_{AIB} while the concentration of D-glutamate was varied. Experimental mixtures consisted of 100 μ M TEA-succinate (pH 7.8), 100 μ M dipotassium succinate, 20 μ M PLP, 1 unit/mL 2°ADH, and 300 μ M NADPH.

decarboxylation (\sim 9%) occurs with L-glutamate in W138F/M141R (data not shown).

End-point assays show that W138F/M141R, W138F, and WT do not use D-glutamate as a substrate. Assays with SSDH find that oxidative decarboxylation does not occur. Likewise, HPLC-based assays to identify GABA, the product of nonoxidative decarboxylation, also find that decarboxylation does not occur with D-glutamate in W138F/M141R. Inhibition studies find that W138F/M141R binds D-glutamate, with a K_i of $89 \pm 10 \text{ mM}$ (Figure 5). In contrast, WT is not inhibited by D-glutamate even at concentrations up to 500 mM (Figure 5).

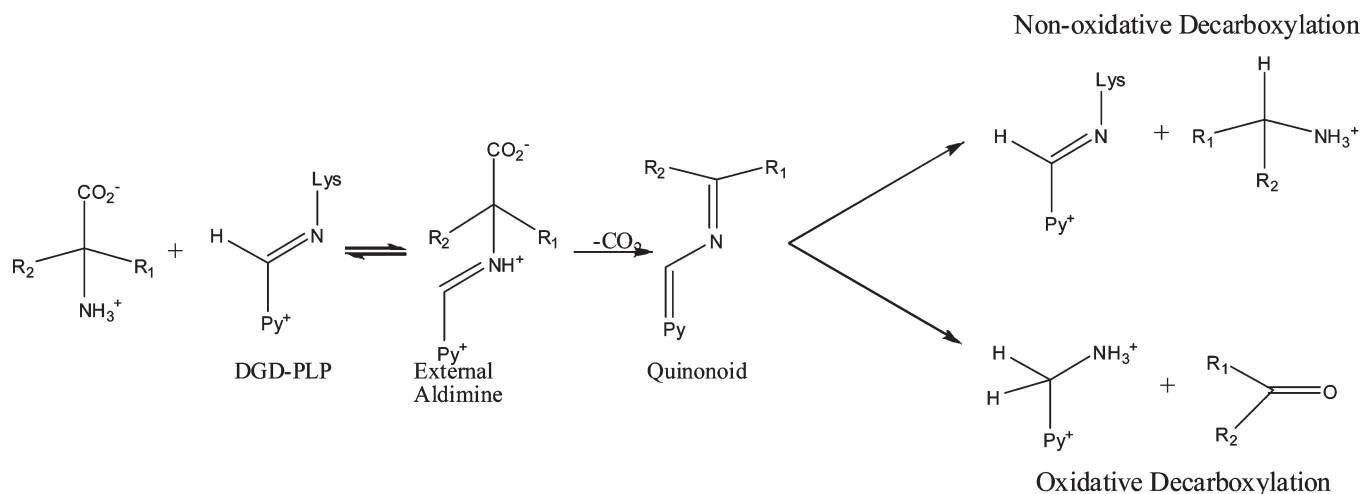
W138F/M141R does not decarboxylate AMG on the basis of end-point assays using 2°ADH. Controls with levulinic acid, the product of oxidative decarboxylation of AMG, show that 2°ADH can use it as a substrate. Inhibition studies find that although W138F/M141R does not decarboxylate AMG, it can bind to the enzyme active site ($K_i = 136 \pm 20 \text{ mM}$).

DISCUSSION

R406 Is Important to Catalysis of Decarboxylation. Decarboxylases often have a hydrophobic active site that destabilizes the charged carboxylate ground state, thereby promoting CO₂ loss. Examples of PLP-dependent decarboxylases that employ this strategy include ornithine decarboxylase (9, 10), dopa decarboxylase (11), and arginine decarboxylase (12). The presence of R406 in the relatively hydrophilic DGD active site is therefore unusual but required of the transamination half-reaction in the normal catalytic cycle. On the basis of the reaction specificity of DGD, it was originally proposed that R406 is necessary for proper substrate binding in the transamination half-reaction but hindered the decarboxylation half-reaction (2). The R406M mutant was expected to relieve the ground-state stabilization R406 affords in the decarboxylation half-reaction and, by this simple reasoning, to increase the decarboxylation rate constant. Although the loss of the interaction between the substrate carboxylate and R406 was expected to weaken substrate binding, the mutation was also expected to shift the binding of the substrate carboxylate to favor the activated A subsite (Figure 1) over the nonactivated B subsite when substrate is bound, thereby increasing k_{decarb} .

As expected, the steady-state results show that substrate binding has been significantly weakened in R406M (Table 1). However,

Scheme 2



the expected increase in the rate of decarboxylation is not observed. Although R406M still maintains the strict specificity for oxidative decarboxylation with AIB observed in WT (3), the steady-state results indicate that decarboxylation is impaired in R406M.

The steady-state results do not rule out the possibility that decarboxylation is rapid but the overall catalytic cycle is limited by slow transamination. To address this possibility, the AIB decarboxylation half-reaction was studied in isolation using the spectral properties of the PLP and PMP cofactors. Although the spectral traces were kinetically complex, these studies clearly show that the maximal rates of the observed processes are not significantly faster than the observed steady-state rate. This rules out the possibility of rapid decarboxylation in R406M and supports a catalytic role for R406 in decarboxylation in addition to substrate binding.

The decarboxylation of alternate substrates in R406M also suggests a catalytic role for R406. The alternate substrates 1-aminocyclopentane-1-carboxylic acid (AC5C) and 1-aminocyclohexane-1-carboxylic acid (AC6C) bind with the cyclic component of their structures in subsites B and C and with the carboxylate in subsite A, based on the X-ray structures of their phosphonate analogues in complex with DGD (13). From the functional model of the DGD active site, one expects these substrates to undergo rapid decarboxylation because the α -carboxylate must occupy the stereoelectronically activated A subsite. However, previous pre-steady-state studies with these substrates found no increase in the decarboxylation rate constant compared to that of AIB (14). This was attributed in part to ground-state stabilization of the α -carboxylate by R406. Removing the positive charge in the R406M mutant was expected to relieve the ground-state stabilization and increase the rate of decarboxylation. Contrary to initial predictions, experiments with these alternate substrates suggest that the R406M mutation does not enhance decarboxylation by removing electrostatic ground-state stabilization from interaction of R406 with the α -carboxylate. In fact, a large decrease in the rate of decarboxylation with AC5C and AC6C compared to that of WT is observed with R406M (Table 2). These results suggest that R406 facilitates decarboxylation.

The reaction with L-alanine also suggests that R406 is important to decarboxylation. In R406M, it was expected that the mutation would increase the portion of substrate bound with its carboxylate in the activated A subsite and therefore increase

the amount of decarboxylation of L-alanine in R406M compared to WT. In contrast to this prediction, no significant amount of decarboxylation, either oxidative or nonoxidative (Scheme 2), occurs in R406M with L-alanine. Instead, L-alanine exclusively undergoes transamination in R406M, supporting the proposal that R406 plays an important role in the catalysis of decarboxylation.

The much larger decreases seen in the rate of decarboxylation with AC5C and AC6C (> 4000-fold) than with AIB (~100-fold) in R406M may be the result of the superposition of two opposing trends in the decarboxylation of AIB and AMS. It is possible that as predicted, AIB and AMS enjoy some degree of rate acceleration due to preferred binding of the substrate carboxylate in the activated A subsite but also suffer from the absence of R406. With the cyclic substrates, there should be no major differences in their orientation and binding between R406M and WT because the cycloalkane occupies subsites B and C. The difference seen in the rate of decarboxylation with these substrates between R406M and WT therefore provides a simpler measure of the effect of the R406M mutation than reactions with either AIB or AMS, which can bind in at least two different conformations in the active site.

A Positive Charge in Position 406 Is Sufficient for Efficient Catalysis. To further elucidate the role of R406, the R406K mutant was made and characterized (Table 1). The K_m values for AIB and AMS increase slightly, further reinforcing the importance of R406 in substrate carboxylate binding. The R406K mutant suggests that a positive charge in the 406 position is required for efficient catalysis in DGD, as shown by a decrease in k_{cat} of only ~10-fold compared to that of WT.

The R406 mutants demonstrate that the simple model in which R406 hinders decarboxylation due to ground-state stabilization is incomplete. Studies with R406K show that the positive charge of a lysine largely rescues the activity lost in the R406M mutant, arguing against a specific role for the guanidino group of R406. In contrast to the original model in which the substrate carboxylate must be completely in the A subsite, interacting only with Q52 and nearly perpendicular to the PLP ring for decarboxylation to occur, the work with the R406 mutants suggests a more subtle catalytic strategy is employed.

It is likely that decarboxylation starts from a position between the A and B subsites, where the substrate carboxylate can enjoy interactions with both R406 and Q52. As the reaction proceeds and negative charge develops on C α , the carboxylate moves into a position more nearly perpendicular to the PLP ring, taking

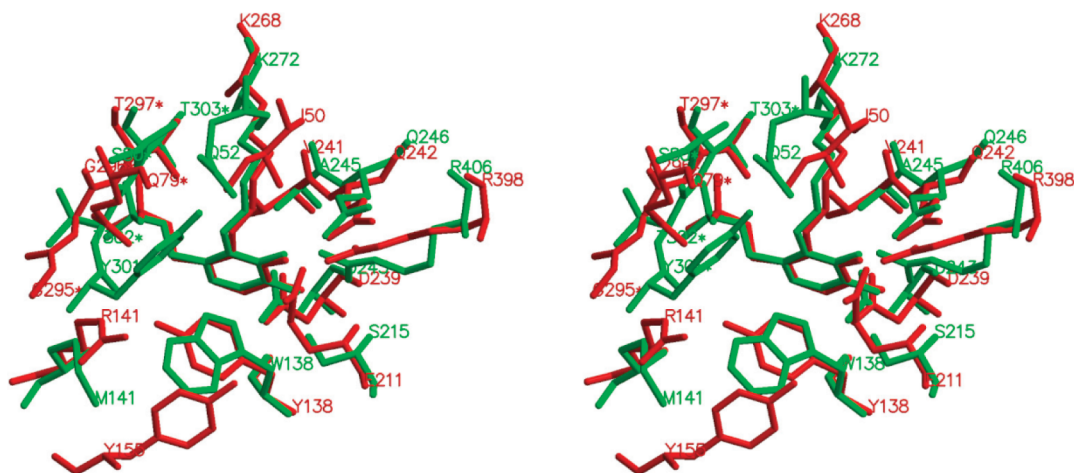


FIGURE 6: Overlay of the active sites of unbound *E. coli* GABA-AT (red) and DGD (green). This figure was prepared with Swiss-PdbViewer and MOLSCRIPT.

advantage of the stabilization that stereoelectronic effects provide as the driving force for such interactions increases. This refined model is supported by X-ray crystallographic studies of DGD in which the phosphonate group of an aminophosphonate inhibitor is found interacting with both R406 and Q52 (13). In this model, the methionine residue in the R406M mutant is unable to hold the substrate carboxylate in an orientation from which decarboxylation can occur, leading to the dramatic decrease in the observed rate of decarboxylation. In contrast, the positive charge of the lysine is sufficient to position the carboxylate between the A and B subsites and efficient catalysis occurs.

W138 Limits the Size of the C Subsite. On the basis of X-ray crystallographic structures (2, 13), it has been proposed that W138 limits the size of the C subsite, making DGD specific for short-chain alkyl groups. Comparison with γ -aminobutyrate aminotransferase (GABA-AT), a related aminotransferase, that binds substrates with longer side chains shows that GABA-ATs have a phenylalanine or tyrosine in the corresponding position (Figure 6). On this basis, the W138F mutation is proposed to open the C subsite, allowing this mutant to bind substrates that place larger side chains in the C subsite.

This prediction is borne out in studies with α -keto acids with increasing side-chain lengths (Figure 3). Compared to that of WT, a smaller decrease in the catalytic efficiency is observed in W138F with an increasing α -keto acid side-chain length. Since an α -keto acid must bind with its side chain in the C subsite, this demonstrates a less restrictive C subsite in W138F. Enlargement of the C subsite in W138F is further supported by inhibition studies with D-phenylglycine. WT does not bind D-phenylglycine, but the more spacious C subsite in W138F allows D-phenylglycine to bind to the mutant enzyme.

The Combined W138F and M141R Mutations Introduce New Substrate Specificity. The W138F/M141R mutant was made to redesign the C subsite, using GABA-AT as a model to introduce new substrate specificity for D-glutamate. It was thought that the mutations would anchor the D-glutamate side chain in the redesigned C subsite (Figure 7A), placing the carboxylate in the activated A subsite from which decarboxylation would occur. L-Glutamate would also bind to the enzyme with the substrate side chain in the redesigned C subsite, but the stereochemistry would require the carboxylate to occupy the B subsite; therefore, decarboxylation was not expected to occur with L-glutamate.

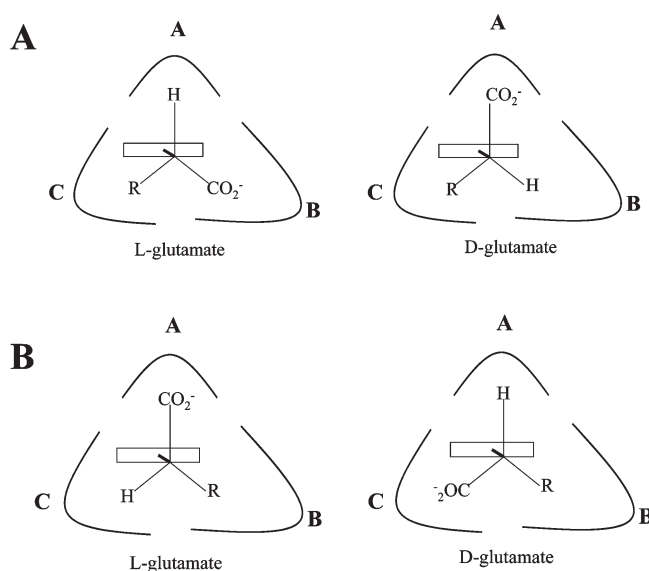


FIGURE 7: Diagram of different binding conformations of L- and D-glutamate in the DGD active site. (A) Expected binding of L- and D-glutamate in the W138F/M141R active site. (B) Revised model of L- and D-glutamate binding in the W138F/M141R active site based on the results presented here.

Steady-state assays show unexpected reactivities for D- and L-glutamate. The double mutant does not decarboxylate D-glutamate, although inhibition studies with D-glutamate show that it can bind to the mutant enzyme. However, W138F/M141R can decarboxylate L-glutamate. It has been shown that decarboxylation occurs from the stereoelectronically activated A subsite in DGD (3) and that stereoelectronic effects accelerate the rate of decarboxylation by at least 6 orders of magnitude compared to the rate of decarboxylation that occurs without the benefit of stereoelectronic stabilization (15). Combined with the reactivity of L- and D-glutamate, this strongly suggests that these substrates are not binding with the glutamate side chain anchored in the redesigned C subsite in W138F/M141R DGD, as initially expected.

A model consistent with the structural and experimental data is shown in Figure 7B. In this model, the glutamate side chain binds in the B subsite, while the mutations made to the C subsite allow binding of the α -carboxylate. The model is consistent with the observed activity with L-glutamate and the binding but lack of

activity with D-glutamate. Both L- and D-glutamate bind with the side chain in the B subsite. With L-glutamate, this places the α -carboxylate in the A subsite. However, with the side chain anchored in the B subsite, D-glutamate binds with the α -carboxylate in the redesigned C subsite, a position that is not activated, and therefore, decarboxylation does not occur. Modeling of W138F/M141R suggests that the α -carboxylate can interact with the positively charged side-chain R141 in the C subsite.

This model makes several predictions that are supported by experiment. The first is that WT does not bind D-glutamate, since the W138F and M141R mutations confer the ability to bind the α -carboxylate in the C subsite. Indeed, there is no significant inhibition seen with D-glutamate up to concentrations of 500 mM. The model also predicts that WT can bind L-glutamate, placing the side-chain carboxylate in the B subsite. Experimentally, it is found that L-glutamate binds to the enzyme with a K_i of 480 mM. The tighter binding of L-glutamate to W138F/M141R compared to WT may be related to the increase in the rate of L-glutamate decarboxylation in the double mutant compared to WT. Although W138F/M141R is able to use L-glutamate as a substrate, it is not efficient in its use of this substrate ($k_{\text{cat}} = 0.0022 \text{ s}^{-1}$, and $k_{\text{cat}}/K_m \text{ L-Glu} = 0.08 \text{ M}^{-1} \text{ s}^{-1}$). The changes have, however, led to significant changes in substrate specificity. An ~ 1000 -fold increase in L-glutamate decarboxylation efficiency is observed for W138F/M141R compared to WT, and the specificity of the redesigned enzyme for L-glutamate has increased by approximately 8 orders of magnitude in the mutant.

Dunathan (*J*) hypothesized that a given PLP-dependent enzyme maintains its reaction specificity by maintaining a specific orientation of the common external aldimine intermediate, aligning the scissile bond parallel to the p orbitals of the extended π system and thereby maximizing orbital overlap and resonance interactions with the activated bond (see the position labeled A in Figure 1). The binding constraints that control the orientation of the substrate in the active site contribute to both reaction specificity and substrate specificity. The interrelation between reaction and substrate specificity is underlined by the work presented here with the R406 mutants. These mutants confirm the importance of R406 in substrate binding and also demonstrate the importance of the positive charge R406 provides in decarboxylation catalysis. Although W138 is not directly involved in catalysis, studies with α -keto acids and the W138F mutant show that this residue limits the size of the C subsite binding pocket, providing specificity for 2,2-dialkylglycines. Finally, by changing two residues, W138F and M141R, we created a mutant enzyme with expanded substrate specificity. In W138F/M141R, the specificity for L-glutamate compared to that for the natural substrate AIB has increased by

approximately 8 orders of magnitude compared to that of the WT enzyme.

REFERENCES

- Dunathan, H. C. (1966) Conformation and Reaction Specificity in Pyridoxal Phosphate Enzymes. *Proc. Natl. Acad. Sci. U.S.A.* 55, 712–716.
- Toney, M. D., Hohenester, E., Keller, J. W., and Jansonius, J. N. (1995) Structural and Mechanistic Analysis of Two Refined Crystal Structures of the Pyridoxal Phosphate-Dependent Enzyme Dialkylglycine Decarboxylase. *J. Mol. Biol.* 245, 151–179.
- Sun, S., Zabinski, R. F., and Toney, M. D. (1998) Reactions of Alternate Substrates Demonstrate Stereoelectronic Control of Reactivity in Dialkylglycine Decarboxylase. *Biochemistry* 37, 3865–3875.
- Sambrook, J., and Russell, D. W. (2001) Molecular Cloning: A Laboratory Manual, 3rd ed., Cold Spring Harbor Laboratory Press, Plainview, NY.
- Liu, W., Peterson, P. E., Langston, J. A., Jin, X., Zhou, X., Fisher, A. J., and Toney, M. D. (2005) Kinetic and Crystallographic Analysis of Active Site Mutants of *Escherichia coli* γ -Aminobutyrate Aminotransferase. *Biochemistry* 44, 2982–2992.
- Christenson, S. D., Wu, W., Spies, M. A., Shen, B., and Toney, M. D. (2003) Kinetic Analysis of the 4-Methylideneimidazole-5-One-Containing Tyrosine Aminomutase in Eneidyne Antitumor Antibiotic C-1027 Biosynthesis. *Biochemistry* 42, 12708–12718.
- Zhou, X., Kay, S., and Toney, M. D. (1998) Coexisting Kinetically Distinguishable Forms of Dialkylglycine Decarboxylase Engendered by Alkali Metal Ions. *Biochemistry* 37, 5761–5769.
- Malashkevich, V. N., Strop, P., Keller, J. W., Jansonius, J. N., and Toney, M. D. (1999) Crystal Structures of Dialkylglycine Decarboxylase Inhibitor Complexes. *J. Mol. Biol.* 294, 193–200.
- Jackson, L. K., Brooks, H. B., Myers, D. P., and Phillips, M. A. (2003) Ornithine Decarboxylase Promotes Catalysis by Binding the Carboxylate in a Buried Pocket Containing Phenylalanine 397. *Biochemistry* 42, 2933–2940.
- Grishin, N. V., Osterman, A. L., Brooks, H. B., Phillips, M. A., and Goldsmith, E. J. (1999) X-ray Structure of Ornithine Decarboxylase from *Trypanosoma brucei*: The Native Structure and the Structure in Complex with α -Difluoromethylornithine. *Biochemistry* 38, 15174–15184.
- Burkhard, P., Dominici, P., Borri-Voltattorni, C., Jansonius, J. N., and Malashkevich, V. N. (2001) Structural Insight into Parkinson's Disease Treatment from Drug-Inhibited Dopa Decarboxylase. *Nat. Struct. Biol.* 8, 963–967.
- O'Leary, M. H., and Piazza, G. J. (1981) Medium Effects in Enzyme-Catalyzed Decarboxylations. *Biochemistry* 20, 2743–2748.
- Liu, W., Rogers, C. J., Fisher, A. J., and Toney, M. D. (2002) Aminophosphonate Inhibitors of Dialkylglycine Decarboxylase: Structural Basis for Slow Binding Inhibition. *Biochemistry* 41, 12320–12328.
- Sun, S., Bagdassarian, C. K., and Toney, M. D. (1998) Pre-Steady-State Kinetic Analysis of the Reactions of Alternate Substrates with Dialkylglycine Decarboxylase. *Biochemistry* 37, 3876–3885.
- Fogle, E. J., Liu, W., Woon, S. T., Keller, J. W., and Toney, M. D. (2005) Role of Q52 in Catalysis of Decarboxylation and Transamination in Dialkylglycine Decarboxylase. *Biochemistry* 44, 16392–16404.
- Zhou, X., and Toney, M. D. (1999) pH Studies on the Mechanism of the Pyridoxal Phosphate-Dependent Dialkylglycine Decarboxylase. *Biochemistry* 38, 311–320.